Engineering the interface characteristics on the enhancement of field electron emission properties of vertically aligned hexagonal boron nitride nanowalls

Peer-reviewed author version

KAMATCHI JOTHIRAMALINGAM, Sankaran; HOANG, Quang; Srinivasu, K.; Korneychuk, S.; TURNER, Stuart; DRIJKONINGEN, Sien; POBEDINSKAS, Paulius; Verbeeck, J.; Leou, K. C.; Lin, I. N. & HAENEN, Ken (2016) Engineering the interface characteristics on the enhancement of field electron emission properties of vertically aligned hexagonal boron nitride nanowalls. In: PHYSICA STATUS SOLIDI A-APPLICATIONS AND MATERIALS SCIENCE, 213(10), p. 2654-2661.

DOI: 10.1002/pssa.201600233
Handle: http://hdl.handle.net/1942/23003

pss-Header will be provided by the publisher

Engineering the interface characteristics on the enhancement of field electron emission properties of vertically aligned hexagonal boron nitride nanowalls

K. J. Sankaran[*,1,2], D. Q. Hoang[1,2], K. Srinivasu[3], S. Korneychuk[4], S. Turner[4], S. Drijkoningen[1,2], P. Pobedinskas[1,2], J. Verbeeck[4], K. C. Leou[3], I. N. Lin[5] and K. Haenen[*,*1,2]

[1] Institute for Materials Research (IMO), Hasselt University, 3590 Diepenbeek, Belgium.

[2] IMOMEC, IMEC vzw, 3590 Diepenbeek, Belgium.

[3] Department of Engineering and System Science, National Tsing Hua University, 30013 Hsinchu, Taiwan.

[4] Electron Microscopy for Materials Science (EMAT), University of Antwerp, 2020 Antwerp, Belgium.

[5] Department of Physics, Tamkang University, 251 Tamsui, Taiwan.

Received ZZZ, revised ZZZ, accepted ZZZ
Published online ZZZ (Dates will be provided by the publisher.)

Keywords hexagonal boron nitride nanowalls, nanocrystalline diamond, Au, field electron emission properties

* Corresponding authors: e-mail sankaran.kamatchi@uhasselt.be, Phone: ++32 11 26 81 11, Fax: ++32 11 268899
** e-mail ken.haenen@uhasselt.be, Phone: ++32 11 268875, , Fax: ++32 11 268899

Utilization of Au and nanocrystalline diamond (NCD) as interlayers noticeably modifies the microstructure and field electron emission (FEE) properties of hexagonal boron nitride nanowalls (hBNNWs) grown on Si substrates. The FEE properties of hBNNWs on Au could be turned on at a low turn-on field of 14.3 V/μm, attaining FEE current density of 2.58 mA/cm^2 and life-time stability of 105 min. Transmission electron microscopy reveals that the Au-interlayer nucleates the hBN directly, preventing the formation of amorphous boron nitride (aBN) in the interface, resulting in enhanced FEE properties. But Au forms as droplets on the Si substrate forming again aBN at the interface. Conversely, hBNNWs on NCD shows superior in life-time stability of 287 min although it possesses inferior FEE properties in terms of largerr turn-on field and lower FEE current density as compared to that of hBNNWs-Au. The uniform and continuous NCD film on Si also circumvents the formation of aBN phases and allows hBN to grow directly on NCD. Incorporation of carbon in hBNNWs from the NCD-interlayer improves the conductivity of hBNNWs, which assists in transporting the electrons efficiently from NCD to hBNNWs that results in better field emission of electrons with high life-time stability.

1 Introduction Evolution of cold cathodes with eminent performance such as low turn-on field, high emission current density and long life-time is strongly preferred for application to field emission displays and vacuum microelectronic devices [1]. Recent interest has been devoted to diamond [2], aluminum nitride [3], and hexagonal boron nitride (hBN) [4] with negative electron affinity (NEA), and carbon nanotubes with a large field-enhancement factor [5] as a promising nominee for field emitters. Among field emitting materials, hBN is one of the most promising materials for cold cathodes. hBN is a two-dimensional (2D) material where B and N atoms are alternatively placed in a hexagonal ring. In the lattice plane the atoms are bound by strong covalent bonds to form 2D hBN sheets, whilst an interaction within different sheets is weak and governed by van der Waals forces [6, 7]. NEA was detected significantly on the surfaces of hBN when treated in hydrogen or oxygen plasma [8]. There have been numerous studies on the field electron emission (FEE) characteristics of hBN films. It was reported that electrons were emitted at a low electric field

from carbon- [9] and sulphur doped- [10] hBN films. A significant improvement of the field emission characteristics was reported for a graphite nanofiber coated with a hBN nanofilm [11]. Moreover, field emission characteristics of carbon nanotube arrays were much improved by coating with hBN films [12,13].

Apart from the combined role of all intrinsic characteristics of hBN, the hBN-to-substrate interface also affects the FEE behavior significantly. Despite many great efforts, synthesised hBN structures still retain unwanted BN phases, i.e. amorphous boron nitride (aBN) and turbostratic boron nitride (tBN), particularly at the initial stage of thin film growth. The presence of these phases is largely dependent on chemical dynamics at the interface of ionized/neutral particles and substrate surface [14,15]. Improvement of phase purity and adhesion of hBN was implemented by inserting buffer layers between hBN and its underlying substrates [16–19]. Mirakami *et al.* accounted that high-phase purity of hBN films could be achieved on amorphous carbon (a-C) substrates [20]. Employing tetrahedral carbon interlayers facilitated the deposition of adherent hBN films with better crystalline quality than on bare Si substrates [21]. Cubic boron nitride crystal grains on Si substrates also enabled to obtain crystalline hBN films with high emission area and enhanced FEE properties [22].

In this work, we have studied the growth of vertically aligned hBN nanowalls (hBNNWs) on Si using Au or nanocrystalline diamond (NCD) materials as interlayers, and observed marked improvement on the FEE properties of hBNNWs. An in-depth investigation is carried out on the consequence of Au- and NCD-interlayers on the microstructural evolution of the hBNNWs, with special attention to interface characteristics. We propose the possible mechanism through which the Au- and NCD-interlayers enhanced the FEE properties of hBNNWs.

2 Experimental section A home-built unbalanced 13.56 MHz radio frequency (RF) sputtering system has been used for hBNNWs growth [6, 7]. A 3 inch-diameter pyrolytic boron nitride (BN) ceramic target with material purity and mass-density of 99.99% and 1.96×10^3 kg/m^3 was utilized. The sputtering conditions were gas mixture of Ar(51%)/N_2(44%)/H_2(5%) and cathode power of 75 W. The working pressure and target-to-substrate distance were 2.1 $\times 10^{-2}$ mbar and 3 cm, respectively. The substrates used for the growth of hBNNWs were bare Si, Au-coated Si and NCD-coated Si. The bare Si substrates were cleaned using a standard RCA procedure [23]. A 100 nm thick Au layer was deposited on cleaned Si substrates by a dc sputter deposition system (Helix) with a power of 50 W in Ar partial pressure of 5 mTorr. A thin layer of Cr (~ 5 nm) was deposited on Si, prior to Au deposition, to ensure strong adhesion of Au on Si. For NCD film growth, the Si substrates were seeded with a waterbased state-of-the-art colloidal suspension of 5 nm detonation nanodiamonds [24]. The nucleated Si substrates were kept in an ASTeX 6500 series microwave plasma enhanced chemical vapor deposition (MPECVD) reactor for the growth of diamond films. In the growth of NCD films, a gas mixture of CH_4 and H_2 with flow rates of 4 and 396 sccm (CH_4/H_2=1/99), respectively, was excited by 3000 W microwave power. The total pressure in the chamber was maintained at 20 Torr. hBNNWs were then synthesized on these substrates using the RF sputtering system for 1 h. The deposited hBNNWs on bare Si substrates, Au-coated Si and NCD-coated Si are designated as 'hBNNWs-Si', 'hBNNWs-Au' and 'hBNNWs-NCD', respectively.

The surface morphology of hBNNWs was examined using a FEI Quanta 200 FEG scanning electron microscope (SEM). The detailed microstructure of the hBNNWs was analyzed using a JEOL 3000F transmission electron microscope (TEM) operated at 300 kV acceleration voltage for high resolution TEM (HRTEM) and a FEI Titan 'cubed' microscope operated at 300 kV for annular dark field (ADF)-scanning TEM (STEM). The convergence semi-angle α used was 22 mrad and the inner acceptance semi-angle β for ADF-STEM imaging was 22 mrad. The FEE characteristics of the samples were measured with a tunable parallel plate setup, in which the anode was a Mo rod of 2 mm in diameter and the sample-to-anode distance was controlled using a micrometer. The current–voltage characteristics were measured using an electrometer (Keithley 2410) under pressures below 10^{-6} Torr. The area of the Mo rod was utilized for evaluating the FEE current density (J). The FEE parameters were extracted from the acquired J–E curves by using the Fowler-Nordheim (F-N) model [25], where E is the applied field. The intersection of the straight lines extrapolated from the low field and high field segments of the F-N plots, viz. $\ln(J/E^2)$-1/E, was designated as turn-on field (E_0).

3 Results and discussion SEM image of hBNNWS-Si (Fig. 1(a)) clearly reveals the well-separated platelets with bending and crumpling morphology of the material. The hBNNWS-Si platelets are vertically positioned with respect to the substrate surface. The cross-sectional high resolution TEM (HRTEM) image of hBNNWs-Si shown in Fig. 2 illustrates the deposition of hBN on Si first yields an interlayer of aBN and subsequently a tBN with (002) basal planes almost perpendicular to the substrate surface, in agreement with the results reported in literature [26]. The edges of the (002) BN basal planes in tBN layer then serve as nucleation sites for the growth of hBN. The FEE measurements and the F-N plots are shown in Fig. 3(a) and inset of Fig. 3(a), respectively, indicating that the hBNNWs-Si require a large E_0 value of $(E_0)_{hBNNWs\text{-}Si}$ = 40.8 V/μm (closed squares of Fig. 3(b) to turn on the FEE process and reach an FEE current density $(J)_{hBNNWs\text{-}Si}$ of 0.22 mA/cm^2 at an applied field of 100.6 V/μm. Moreover, the life-time stability (τ) measurements shows that the emission current variations of hBNNWs-Si recorded only a period of

25 min at a current density of J=0.20 mA/cm^2, which corresponds to a working field of 99.3 V/μm (open circles of Fig. 3(b)). The hBN material is completely damaged after life-time measurements (Fig. 4(a)). The reason for the inferior FEE behavior of hBNNWs-Si materials is the presence of aBN and tBN in the interface that hinders the transport of electrons crossing the diamond-to-Si interface. Thus, the modification on the interfacial microstructure of hBNNWs is needed to improve their FEE properties. Here, we utilize Au- and NCD- films as interlayers for this purpose.

Table 1 Field electron emission properties of the hBNNWs deposited on Si, Au-coated Si and NCD-coated Si substrates.

materials	turn-on field (E_0) (V/μm)	current density (J) (mA/cm^2)	life-time (τ) (min) @ 0.2 mA/cm^2
hBNNWs-Si	40.8	0.22 @ 100.6 V/μm	25
hBNNWs-Au	14.3	2.58 @ 25.9 V/μm	105
hBNNWs-NCD	30.8	0.57 @ 69.1 V/μm	287

Figures 1(b) and 1(c) show that the utilization of Au- and NCD-interlayers markedly modified the surface morphology of hBNNWs films. For the hBNNWs films grown on Au-coated Si substrates, the hBNNWs grains are uniformly grown on the substrates and they are mutually interconnected forming an extended network. A clear sub-branching phenomenon becomes visible with smaller nanowalls growing on the sides of the larger nanowalls, thus forming a three-dimensional nanostructure network. For hBNNWs-NCD, the hBNNWs formed micron-sized aggregates, which appear to grow on top of each diamond grain of the NCD films separately (Fig. 1(c)). The inset of Fig. 1(c) shows an SEM image of NCD film grown on the Si substrate, indicating that the entire surface of Si was uniformly covered with randomly oriented diamond grains with distinguishable edges and facets and having grain sizes of 0.3–0.8 μm. Fig. 1(c) shows that the surface of the NCD film was uniformly covered with a layer of hBNNWs.

The FEE properties of the hBNNWs were dramatically improved due to the utilization of Au- and NCD- interlayers. The E_0 value decreases to around $(E_0)_{hBNNWs\text{-}Au}$ = 14.3 V/μm, accompanied by an abrupt increase in the FEE current density $(J)_{hBNNWs\text{-}Au}$ = 2.58 mA/cm^2 in an applied field of 25.9 V/μm for hBNNWs-Au (curve II, Fig. 3(a)). Moreover, the hBNNWs-Au achieves a life-time stability of $(\tau)_{hBNNWs\text{-}Au}$ = 105 min at a working current density of J-value of 0.20 mA/cm^2, which corresponds to working field of 20.1 V/μm (open circles of Fig. 3(b)). After life-time measurements, the hBNNWs are damaged forming pits on the substrates (Fig. 4(b)).

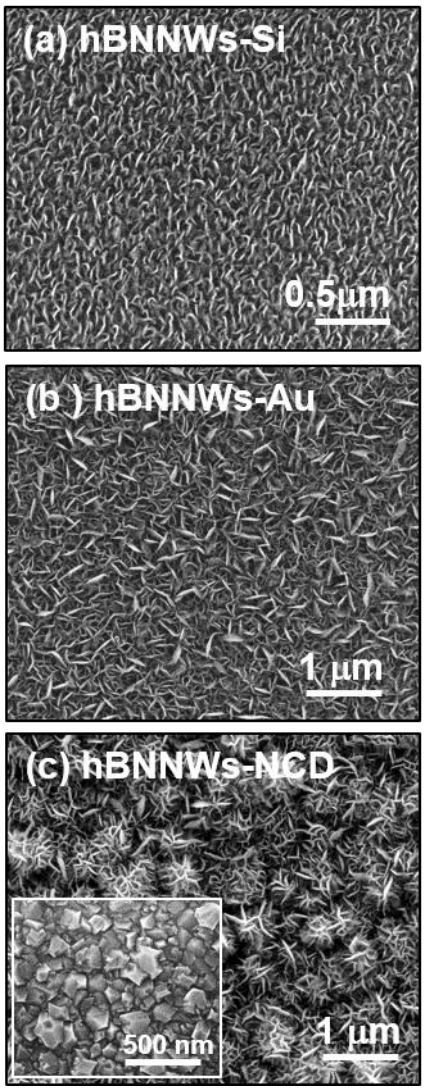

Figure 1 Plane view SEM micrographs of (a) hBNNWs-Si, (b) hBNNWs-Au, and (c) hBNNWs-NCD with inset showing the morphology of NCD films.

On the other hand, curve III in Fig. 3(a) shows that the FEE process for hBNNWs-NCD can be turned on at $(E_0)_{hBNNWs\text{-}NCD}$ = 30.8 V/μm (closed squares of Fig. 2(b)), which is markedly higher than $(E_0)_{hBNNWs\text{-}Au}$ (curve II of Fig. 3(a)). The J value of hBNNWs-NCD can only reach $(J)_{hBNNWs\text{-}NCD}$ = 0.57 mA/cm^2 at an applied field of 69.1 V/μm. The hBNNWs-NCD exhibit significantly higher E_0 and lower J values compared with the values of hBNNWs-Au that are apparently due to the lower electrical conductiv-

ity of the NCD films, which are nominally undoped. Nevertheless, the utilization of NCD as interlayers increased the life-time of the emitters significantly. The life-time stability measurement of hBNNWs-NCD (open circles of Fig. 3(b)) indicates that the emission current variations recorded over a period of 287 min at a working current density of 0.20 mA/cm^{2}corresponding to working field of 59.2 V/μm, which is significantly higher than that of the hBNNWs-Au films and almost 10 times as much that of the hBNNWs-Si films. To facilitate the comparison, the E_0-value and the life-time of these three kinds of hBNNWs films were re-plotted in Fig. 3(b) and these FEE parameters are summarized in Table 1. Importantly, hBNNWs withstand even 287 min of life-time studies (Fig. 4(c)), which discloses the robustness of the hBNNWs-NCD in field emission devices. It is to be noted here that, we have fabricated five hBNNWs-Si, hBNNWs-Au and hBNNWs-NCD samples which were tested in the same configuration at three places of each sample by keeping a constant anode to cathode distance. The data presented in Fig. 3 are the average of the FEE properties of these samples.

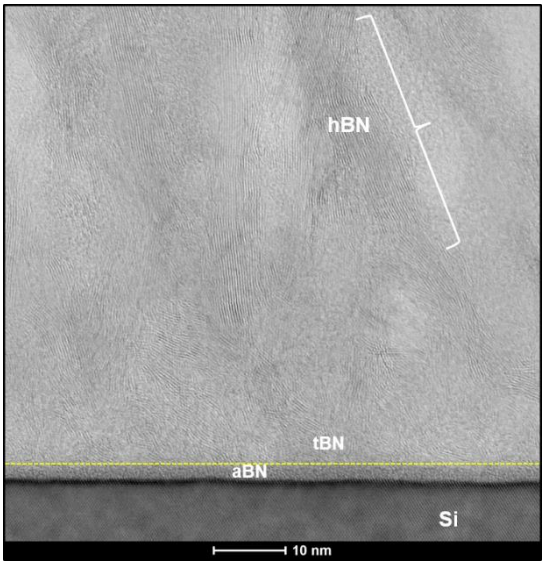

Figure 2 A cross-sectional HRTEM image of hBNNWs-Si. These micrographs show the presence of aBN and tBN sequentially prior to the growth of hBN phase when the hBNNWs were grown directly on Si substrates.

It is apparent that the SEM morphology examination is not able to unambiguously explain the mechanism for the improvement in the FEE properties owing to the utilization of Au and NCD as interlayers. Detailed microstructural examination using TEM is necessary. High-angle annular dark-field (HAADF) image in STEM mode with an HAADF detector was acquired and shown in Fig. 5(a). Notably, in TEM, when the elastically scattered electrons were diffracted incoherently, the scattering angle is closely related to the atomic number of the species involved. The heavier the species are, the larger the scattering angle. An HAADF image is obtained when the incoherently scattered electrons are collected using a high-angle annular detector, which provides information on the elemental distribution of the samples [27,28]. The HAADF image shown in Fig. 5(a) reveals that Au forms as droplets on the surface of the Si substrate due to the Au-Si eutectic reaction and the energetic ions bombardment during the hBNNWs growth process that leads to uneven growth mechanism of hBNNWs-Au. For the regions where the hBNNWs were grown directly on Au droplets, no aBN and tBN phases was formed, but for the regions where the Si was exposed to hBN growing species, aBN/tBN were formed at the interface. Such a growth mechanism will be further analyzed using high resolution STEM (HRSTEM). To illustrate more clearly the elemental distribution of the species near the interface in hBNNWs-Au, the energy dispersive X-ray (EDX) mapping was performed. Fig. 5(b) shows a micrograph composed of the EDX mapping with Si (green), Au (red), Cr (pink) and hBN (black) for the same region depicted in Fig. 5(a). The growth of hBNNWs on Au droplets is clearly illustrated.

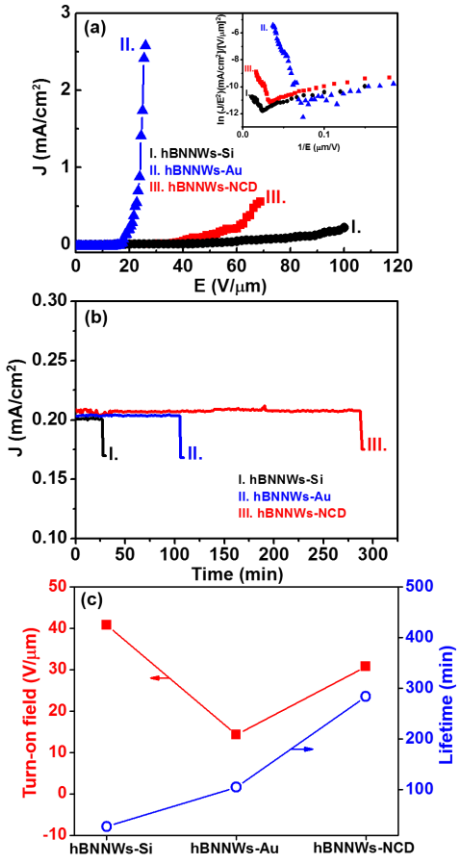

Figure 3 (a) Field electron emission (FEE) current density (J) as a function of applied field (E) of I. hBNNWs-Si, II. hBNNWs-Au, and III. hBNNWs-NCD. The inset in 'a' shows the corresponding Fowler-Nordheim plots. (b) Variation in the turn-on field (E_0, solid squares) and life-time stability (τ, open circles) of hBNNWs grown on Si, Au and NCD.

More detailed investigations were carried out on the identification of different phase constituents in hBNNWs-Au by HRSTEM studies. Fig. 5(c) shows the cross-sectional HRSTEM micrographs of the corresponding region 'A' marked in Fig. 5(a) where the hBNNWs were grown directly on Si. This figure reveals a thin, continuous, and uniform interfacial layer of a few nanometers in thickness (indicated by yellow dotted lines in Fig. 5(c)). In contrast, Fig. 5(d) shows that for the region 'B' marked in Fig. 5(a) (hBN grown on Au) reveals that hBN phases formed directly on the Au droplets obstructing the growth of aBN/tBN in the interface. The FT images, FT_{d1} and FT_{d2}, in Fig. 5(d) highlight hBN and Au in regions 'd1' and 'd2', respectively. There is no aBN layer observed in Fig. 5(d). The above-described results indicate that the presence of a Au-interlayer inhibits the formation of aBN/tBN that transfers the electrons directly from Si to the hBNNWs, resulting in better FEE properties than the hBNNWs-Si. But the interface of hBNNWs-Au/Si is not uniform, some of the regions are more conductive than others which results in non-uniform distribution of FEE current. The preferential deterioration of some contacts is presumably the cause, which lead to short life-time of the hBNNWs-Au.

To unravel the microstructure of the hBNNWs-NCD for understanding how the utilization of NCD-interlayer enhanced the life-time of the emitters, TEM microstructural studies were carried out on this sample. Fig. 6(a) shows a cross-sectional HAADF-STEM micrograph of the hBNNWs-NCD heterostructure, in which the hBNNWs and NCD regions are clearly marked. To further explore the detailed elemental distribution, energy-filtered B, N and C maps, which are EDX-STEM images of the hBNNWs-NCD, were constructed and superimposed (Fig. 6(b)).

It can be seen from Fig. 6(b) that, in contrast to the uniform distributions of B and N in hBNNWs and carbon in diamond regions, there was C (green) enrichment at the interface region between diamond (blue) and hBN (red) and within some internal areas of hBN. It is clear from the maps that some carbon has been incorporated into the hBN structures. From the HRSTEM image shown in Fig. 6(c) for hBNNWs-NCD, it can be assured that the hBNNWs grow directly on the diamond surfaces, without the formation of any precursor layers like aBN or tBN prior to its nucleation. Highly ordered lattice fringes of hBNNWs can be observed, indicating that the hBNNWs are well crystallized. Moreover, the insets reveal the diamond (D) grain region (region c1, FT_{c1}) and the hBN region (region c2, FT_{c2}), respectively.

In Fig. 6(d), two summed EELS spectra from the diamond and the hBN regions are plotted. The carbon K-edge spectrum (spectra I of Fig. 6(d)) acquired from the diamond region (region c1 of Fig. 6(c)) is typical of sp^3-carbon, with a strong σ^* contribution at 292 eV and deep valley in 302 eV.[29,30] The EELS spectrum (spectra II of Fig. 6(d)) corresponding to the hBN region (region c2 of Fig. 6(c)) exhibits two distinct edges; the boron-K 188 eV and the nitrogen-K at 401 eV.[31–33] The fine structure of the B-K and N-K edges are typical of the sp^2-coordinated layered BN, indicating that the obtained nanowalls are BN with the hexagonal layered structure. As mentioned above, in addition to the core-loss K-edges of B and N, the residual presence of carbon is also detected through presence of a core-loss carbon-K edge at 284 eV (π^* band). The fine structure of the carbon K-edge is typical of a-C, confirming that C species are incorporated into the hBN. These results are in agreement with the findings from Leung *et al.*, where they observed the diffusion of C in the interface during the growth of cubic BN on amorphous tetrahedral carbon interlayers [34].

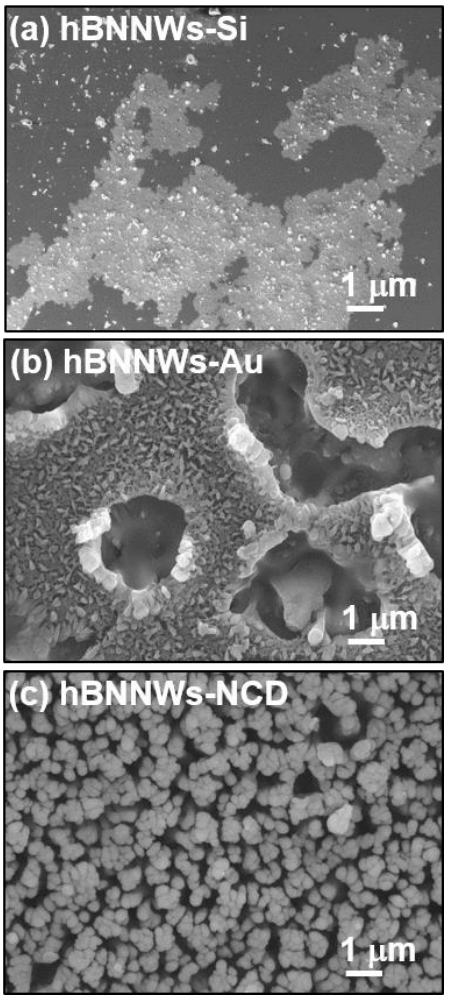

Figure 4 Plane view SEM micrographs of (a) hBNNWs-Si, (b) hBNNWs-Au, and (c) hBNNWs-NCD after FEE life-time measurements.

The presence of C in the interface region is possibly induced by carbon incorporation and dynamic recoil ion mixing in an early stage of boron nitride deposition. This incorporated carbon region then corresponds to a C-B-N

gradient layer, which may contribute on the interfacial stress relaxation and the improved FEE properties of hBNNWs-NCD films.

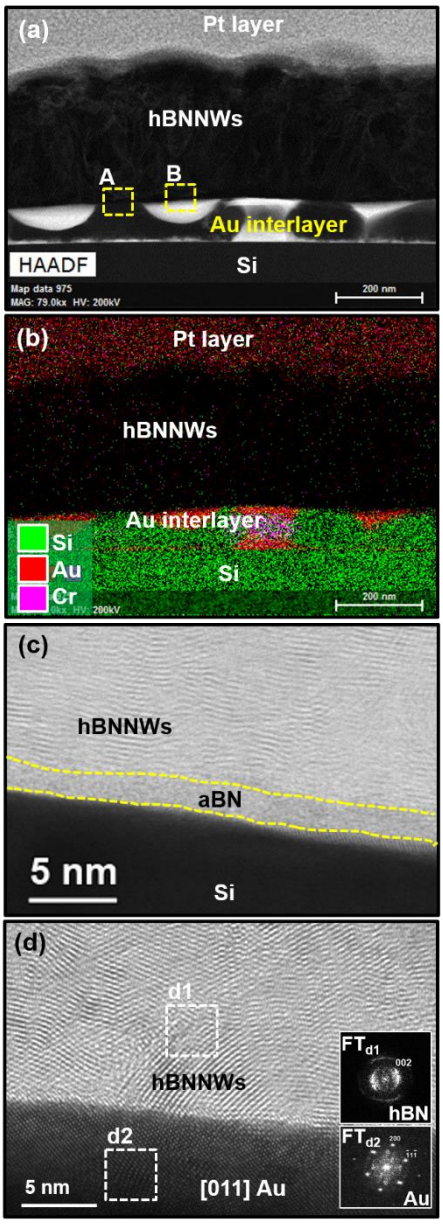

Figure 5 (a) Cross-sectional HAADF-STEM image of hBNNWs-Au. (b) EDAX-STEM mapping of the regions corresponding to (a). (c) and (d) High resolution BF-STEM image of the hBNNWs-Au corresponding to regions A and B of (a), respectively. The insets FT_{d1} and FT_{d2} show the FT images corresponding to regions d1 and d2, respectively.

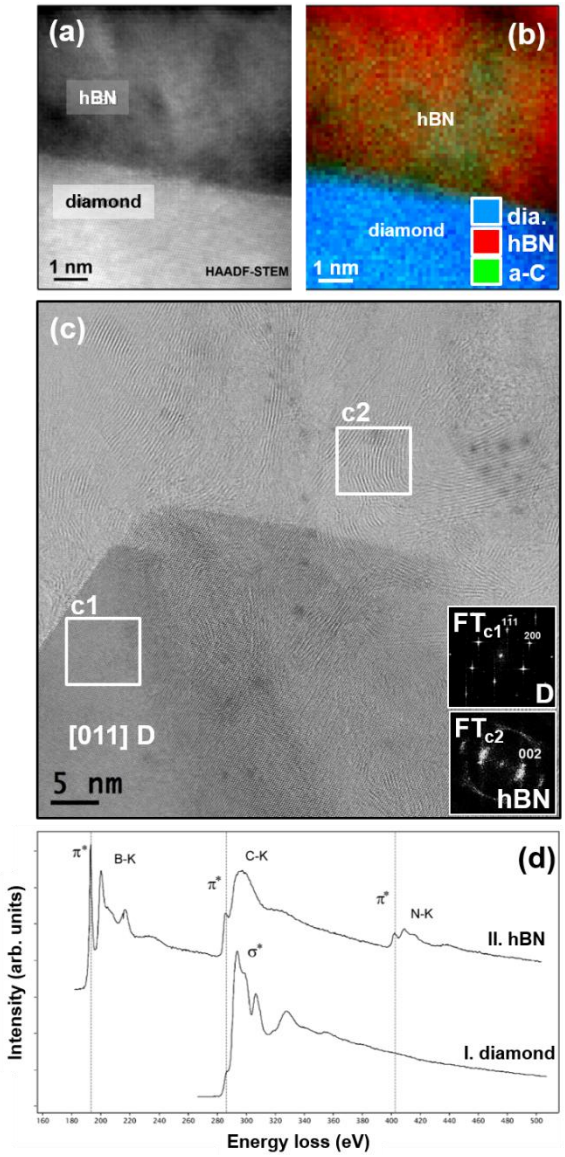

Figure 6 (a) Cross-sectional HAADF-STEM image of hBNNWs-NCD and (b) EDAX-STEM mapping of the regions corresponding to (a). (c) High resolution STEM image of hBNNWs-NCD. The insets FT_{c1} and FT_{c2} show the FT images corresponding to regions c1 and c2, respectively. (d) Summed EELS core-loss spectra taken from the diamond and hBN regions.

Now, the question to be answered is how the utilization of a NCD interlayer possible assists in enhancing the field emission properties, especially the longer life-time for hBNNWs-NCD? It is obvious from the HRSTEM image (Fig. 6(c)) that hBNNWs nucleated and grew directly on the NCD surface inhibiting the formation of aBN/tBN phases at the interface that eliminate the formation of a resistive layer for transporting the electrons. Additionally, when doped with carbon, hBN exhibited semiconducting properties due to the appearance of dopants or defect states in the bandgap [36, 37]. Both factors improved the FEE properties of the

hBNNWs-NCD, although the NCD layer is quite resistive limiting the FEE behavior attainable for these films. Concerning the mechanism which enhanced the life-time of the hBNNWs-NCD films owing to the utilization of NCD as interlayer, it is evident that the elimination of the aBN/tBN interface phase is the main factor. The NCD is stable and will not be degraded even though the FEE current might heat up the film. Moreover, the high thermal conductivity of NCD films [38] is expected to be beneficial in heat spreading and will improve the life-time stability of the hBNNWs-NCD films. Utilization of NCD films which are more conductive might further improve the overall FEE properties of hBNNWs-NCD films.

4 Conclusions In summary, we engineered the interface characteristics of hBNNWs using Au and NCD as interlayers that markedly modified the interfacial microstructure and enhanced the FEE properties of the hBNNWs. Employing a Au interlayer markedly enhances the FEE properties for hBNNWs, viz. low E_0 of 14.3 V/μm with a high FEE J of 2.6 mA/cm^2 (at an applied field of 26.0 V/μm) and better τ value up to a period of 105 min, than those of the FEE properties of hBNNWs grown directly on Si (E_0=40.8 V/μm, J=0.22 @ 100.6 V/μm and τ=25 min). Cross-sectional TEM investigations reveal that the Au interlayer circumvents the formation of aBN and tBN prior to the hBN growth that effectively improves the electron transport from Si to hBNNWs. But Au forms as droplets on the surface of Si which leads to non-uniformity in interface structure and thus resulted in non-satisfactory life-time. On the other hand, hBNNWs grown on a NCD interlayer, although possess inferior FEE properties in terms of E_0 (30.8 V/μm) and J (0.57 @ 69.1 V/μm) values, resulted in superior in life-time stability of 287 min as compared to the hBNNWs grown on Au-interlayer. The NCD interlayer circumvents the formation of aBN and forms a uniform interface that allows stable electron transport from Si to the hBNNWs, resulting in higher life-time stability of hBNNWs than those of hBNNWs-Au films.

It is expected using UNCD films, which were grown in CH_4/Ar plasma and were more conductive than NCD films, as interlayer, replacing the NCD interlayer, can possibly lower the turn-on field for hBNNWs materials. However, the risk is that the UNCD films are much softer than the NCD films and might be damaged by the DC plasma during the growth of hBNNWs materials. The other probable approach is to dope NCD films converting them into highly conductive interface layer.

Acknowledgements The authors like to thank the financial support of the Research Foundation Flanders (FWO) via Research Project G.0456.12 and the Methusalem "NANO" network. K. J. Sankaran, P. Pobedinskas and S. Turner are FWO Postdoctoral Fellows of the Research Foundations– Flanders (FWO).

References

[1] K. Subramanian, Y. M. Wong, W. P. Kang, J. L. Davidson, B. K. Choi, and M. Howell, Diamond and Relat. Mater. **16**, 1997 (2007).

[2] K. J. Sankaran, B. R. Huang, A. Saravanan, D. Manoharan, N. H. Tai, and I. N. Lin, ACS Appl. Mater. Interfaces **7**, 27078 (2015).

[3] Q. Wu, N. Liu, Y. Zhang, W. Qian, X. Wang, and Z. Hu, J. Mater. Chem. C **3**, 1113 (2015).

[4] T. Sugino, C. Kimura, and T. Yamamoto, Appl. Phys. Lett. **80**, 3602 (2002).

[5] E. Minoux, O. Groening, K. B. K. Teo, S. H. Dalal, L. Gangloff, J. P. Schnell, L. Hudanski, I. Y. Y. Bu, P. Vincent, P. Legagneux, G. A. J. Amaratunga, and W. I. Milne, Nano Lett. **5**, 2135 (2005).

[6] B. BenMoussa, J. D'Haen, C. Borschel, J. Barjon, A. Soltani, V. Mortet, C. Ronning, M. D'Olieslaeger, H.-G. Boyen, and K. Haenen, J. Phys. D: Appl. Phys. **45**, 135302 (2012).

[7] D. Q. Hoang, P. Pobedinskas, S. S. Nicley, S. Turner, S. D. Janssens, M. K. Van Bael, J. D'Haen, and K. Haenen, Cryst. Growth Des. **16**, 3699 (2016).

[8] M. J. Powers, M. C. Benjamin, L. M. Porter, R. J. Nemanich, R. F. Davis, J. J. Cuomo, G. L. Doll, and S. J. Harris, Appl. Phys. Lett. **67**, 3912 (1995).

[9] R. W. Pryor, Appl. Phys. Lett. **68**, 1802 (1996).

[10] T. Sugiono, S. Kawasaki, K. Tanioka, and J. Shirafuji, Appl. Phys. Lett. **71**, 2704 (1997).

[11] T. Sugiono, T. Yamamoto, C. Kimura, H. Murakami, and M. Hirakawa, Appl. Phys. Lett. **80**, 3808 (2002).

[12] X. Yang, Z. Li, F. He, M. Liu, B. Bai, W. Liu, X. Qiu, H. Zhou, C. Li, and Q. Dai, Small, **11**, 3710 (2015).

[13] H. C. Chang, H. J. Tsai, W. Y. Lin, Y. C. Chu, and W. K. Hsu, ACS Appl. Mater. Interfaces, **7**, 14456 (2015).

[14] A. Pakdel, Y. Bando, and D. Golberg, Chem. Soc. Rev. **43**, 934 (2014).

[15] D. R. McKenzie, W. D. McFall, S. Reisch, B. W. James, I. S. Falconer, R. W. Boswell, H. Persing, A. J. Perry, and A. Durandet, Sur. Coat. Tech. **78**, 255 (1996).

[16] P. B. Mirkarimi, D. L. Medlin, and K. F. McCarty, Appl. Phys. Lett. **66**, 2813 (1995).

[17] Y. K. Yap, T. Aoyama, Y. Wada, M. Yoshimura, Y. Mori, and T.Sasaki, Diamond Relat. Mater. **9**, 592 (2000).

[18] W. Otanõ-Rivera, R. Messier, L. J. Pilione, J. J. Santiago, and G. Lamaze, Diamond Relat. Mater. **13**, 1690 (2004).

[19] D. G. Kvashnin, A. V. Krasheninnikov, D. Shtansky, P. B. Sorokin, and D. Golberg, Phys. Chem. Chem. Phys. **18**, 965 (2016).

[20] P. B. Mirkarimi, K. F. McCarty, G. F. Cardinale, D. L. Medlin, D. K. Ottesen, H. A. Johnsen, J. Vac. Sci. Technol. A **14**, 251 (1996).

[21] K. M. Leung, C. Y. Chan, Y. M. Chong, Y. Yao, K. L. Ma, I. Bello, W. J. Zhang, and S. T. Lee, J. Phys. Chem. B **109**, 16272 (2005).

[22] C. Kimura, T. Yamamoto, T. Sugino, J. Vac. Sci. Technol. B **19**, 1051 (2001).

[23] G. K. Celler, D. L. Barr, and J. M. Rosamilia, Electrochem. Solid-State Lett. **3**, 47 (2000).
[24] O. A. Williams, O. Douheret, M. Daenen, K. Haenen, E. Osawa, and M. Takahashi, Chem. Phys. Lett. **445**, 255 (2007).
[25] R. H. Fowler, and L. Nordheim, Proc. R. Soc. London, Ser. A **119**, 173 (1928).

[26] P. B. Mirkarimi, K. F. McCarty, and D. L.Medlin, Mater. Sci. Eng. **R21**, 47 (1997).
[27] P. A. Midgley, and M. Weyland, Ultramicroscopy **96**, 413 (2003).
[28] S. Bals, G. Van Tendeloo, and C. Kisielowski, Adv. Mater. **18**, 892 (2006).
[29] A. Politano, and G. Chiarello, Gold Bulletin **42**, 195 (2009).

[30] D. Zhou, T. G. McCauley, L. C. Qin, A. R. Krauss, and D. M. Gruen, J. Appl. Phys. **83**, 540 (1998).
[31] A. Loiseau, F. Willaime, N. Demoncy, G. Hug, and H. Pascard, Phys. Rev. Lett. **76**, 4737 (1996).
[32] M. Terrones, W. K. Hsu, H. Terrones, J. P. Zhang, S. Ramos, J. P. Hare, R. Castillo, K. Prassides, A. K. Cheetham, H. W. Kroto, and D. R. M. Walton, Chem. Phys. Lett. **259**, 568 (1996).
[33] W. Q. Han, Y. Bando, K. Kurashima, and T. Sato, Appl. Phys. Lett. **73**, 3085 (1998).
[34] K. M. Leung, C. Y. Chan, Y. M. Chong, Y. Yao, K. L. Ma, I. Bello, W. J. Zhang, and S. T. Lee, J. Phys. Chem. B **109**, 16272 (2005).
[35] Z. Remes, M. Nesládek, K. Haenen, K. Watanabe, and T. Taniguchi, Phys. Status Solidi A **202**, 2229 (2005).

[36] X. Wei, M. S. Wang, Y. Bando, and D. Golberg, ACS Nano **5**, 2916 (2011).
[37] T. M. Schmidt, R. J. Baierle, P. Piquini, and A. Fazzio, Phys. Rev. B **67**, 113407 (2003).
[38] J. Sermeus, B. Verstraeten, R. Salenbien, P. Pobedinskas, K. Haenen, and C. Glorieux, Thin Solid Films **590**, 284 (2015).